Insight into the reactive properties of newly synthesized 1,2,4-triazole derivative by combined experimental (FT-IR and FR-Raman) and theoretical (DFT and MD) study

Accepted Manuscript

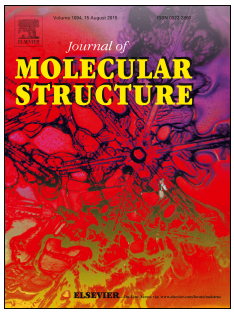

Insight into the reactive properties of newly synthesized 1,2,4-triazole derivative by combined experimental (FT-IR and FR-Raman) and theoretical (DFT and MD) study

Y. Sheena Mary, Fatmah A.M. Al-Omary, Gamal A.E. Mostafa, Ali A. El-Emam, P.S. Manjula, B.K. Sarojini, B. Narayana, Stevan Armaković, Sanja J. Armaković, C. Van Alsenoy

PII: S0022-2860(17)30429-5

DOI: 10.1016/j.molstruc.2017.04.001

Reference: MOLSTR 23618

To appear in: *Journal of Molecular Structure*

Received Date: 10 October 2016

Revised Date: 18 March 2017

Accepted Date: 3 April 2017

Please cite this article as: Y.S. Mary, F.A.M. Al-Omary, G.A.E. Mostafa, A.A. El-Emam, P.S. Manjula, B.K. Sarojini, B. Narayana, S. Armaković, S.J. Armaković, C. Van Alsenoy, Insight into the reactive properties of newly synthesized 1,2,4-triazole derivative by combined experimental (FT-IR and FR-Raman) and theoretical (DFT and MD) study, *Journal of Molecular Structure* (2017), doi: 10.1016/j.molstruc.2017.04.001.

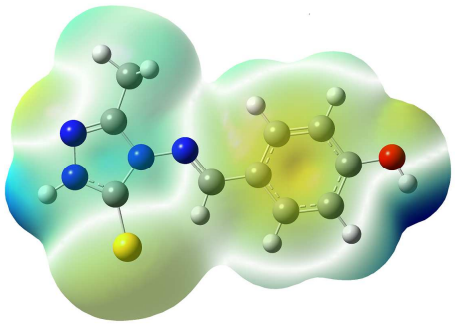

Insight into the reactive properties of newly synthesized 1,2,4-triazole derivative by combined Experimental (FT-IR and FR-Raman) and theoretical (DFT and MD) study

Sheena Mary Y[a*], Fatmah A. M. Al-Omary[b], Gamal A. E. Mostafa[b], Ali A. El-Emam[b], P.S.Manjula[c], B.K.Sarojini[d], B.Narayana[e], Stevan Armaković[f], Sanja J. Armaković[g], C.Van Alsenoy[h]

[a]Department of Physics, Fatima Mata National College, Kollam, Kerala, India

[b] Department of Pharmaceutical Chemistry, College of Pharmacy, King Saud University, Riyadh 11451, Saudi Arabia

[c]Department of Chemistry, P.A.College of Engineering Mangalore, Nadupadavu, Mangaluru, Karnataka , India

[d]Department of Industrial Chemistry, Mangalore University, Mangalagangothri, Mangaluru, Karnataka, India

[e]Department of Chemistry, Mangalore University, Mangalagangothri, Mangaluru, Karnataka, India

[f]University of Novi Sad, Faculty of Sciences, Department of Physics,
Trg D. Obradovića 4, 21000 Novi Sad, Serbia

[g]University of Novi Sad, Faculty of Sciences, Department of Chemistry, Biochemistry and Environmental Protection, Trg D. Obradovića 3, 21000 Novi Sad, Serbia

[h]Department of Chemistry, University of Antwerp, Groenenborgerlaan 171, B-2020, Antwerp, Belgium

Author for correspondence: email: sypanicker@rediffmail.com

Abstract

The vibrational spectral analysis has been carried out on 4-[(*E*)-(4-hydroxybenzylidene)amino]-3-methyl-1*H*-1,2,4-triazole-5(4*H*)-thione (HBAMTT) in order explore the chemical and pharmacological properties. The most important reactive sites have been identified employing molecular electrostatic potential map. Nonlinear optical properties are identified and the first hyperpolarizability is 80.35 times that of urea, which is standard NLO material. The molecular activity is studied from the dislocation of the frontier molecular orbitals and NBO analysis is

carried to gain an insight into the charge transfer within the molecular system. Using molecular electrostatic potential map, the electrophilic and nucleophilic sites are identified. Title molecule was further investigated from the aspect of local reactivity properties by calculations of average local ionization energies (ALIE) and Fukui functions. Vulnerability towards autoxidation and hydrolysis mechanisms has been assessed thanks to the calculations of bond dissociation energies (BDE) and radial distribution functions (RDF), respectively. This information was also valuable for the initial investigation of degradation properties of the title molecule. Thanks to the molecular docking studies, it can be concluded that docked ligand forms a stable complex with AChE and could be used as a new drug for the Alzheimer's disease, myasthenia gravis and glaucoma.

Keywords: Triazole; average local ionization energy; radial distribution; density functional theory; molecular docking.

1. Introduction

Schiff bases have found wide analytical applications and metal coordination [1,2] and possess antihypertensive, anti-inflammatory [3], analgesic [4], sedative [5] and fungicidal [6] activities. In the literature several 1,2,4-triazole derivatives were reported to possess potent antimicrobial [7-10] and anti-inflammatory activities [11-13], while vibrational spectroscopic studies of 1,2,4-triazole derivatives are reported in literature recently [14,15]. Due to the high stability organic pharmaceutical molecules are hardly degraded under natural conditions [16]. Frequent and improper usages eventually lead to their presence in all types of water throughout the world, where they exhibit toxic effects towards aquatic organisms [16,17]. Their presence in water resources is very upsetting for scientific community who needs to seek other ways for their efficient removal, since conventional approaches turned out to be ineffective [18,19]. Methods for the removal of organic pharmaceutical molecules based on the forced degradation with advanced oxidation processes are efficient and could be the good choice as an alternative, however further developments are necessary [17,18,20-24]. Alternative methods for purification of water are complicated and there are still many challenges that need to be solved, but optimization and rationalization of these procedures can be achieved by employing the DFT calculations and molecular dynamics (MD) simulations [25-28]. These computational experiments allow anticipation of reactive properties of investigated molecules, thus enabling the scientists to cut down expenses related to tedious experiments. In the present work, the

vibrational spectroscopic analysis, molecular dynamics simulations to understand various properties and molecular docking studies of the title molecule, 4-[(*E*)-(4-hydroxybenzylidene)amino]-3-methyl-1*H*-1,2,4-triazole-5(4*H*)-thione (HBAMTT) are reported.

2. Experimental details

The title compound, 4-[(*E*)-(4-hydroxybenzylidene)amino]-3-methyl-1*H*-1,2,4-triazole-5(4*H*)-thione was synthesized as reported in literature [29]. 4-Amino-5-methyl-2,4-dihydro-3H-1,2,4-triazole-3-thione (0.01 mol, 1.3g) was added to a suspension of 4-hydroxy benzaldehyde (1.22g, 0.01 mol) in ethanol (15 ml), and heated to get a clear solution and then a few drops of conc. H_2SO_4 was added as a catalyst and refluxed for 36 hr. on a water bath. The precipitate formed was filtered and re-crystallized from methanol to get the title compound. The FT-IR spectrum (Fig. 1) and FT-Raman spectrum (Fig. 2) were recorded using KBr pellets on DR/Jasco FT-IR spectrometer and Bruker RFS 100/s, Germany.

3. Computational details

Calculations of the title compound were carried out with the Gaussian09 program [30] using B3LYP/6-311++G(d) (5D, 7F) basis set to predict the molecular structure and wavenumbers and a scaling factor of 0.9613 had to be used for obtaining a considerably better agreement with experimental data [31]. Structural parameters with XRD data corresponding to the optimized geometry of the title compound (Fig. 3) are given in Table S1 (supporting material). The assignments of the calculated frequencies are done using Gaussview [32] and GAR2PED [33] software. The natural bond orbitals (NBO) calculations were performed using NBO 3.1 program [34] as implemented in the Gaussian09 and the important interactions are tabulated in tables 1 and S2 (supporting material).

DFT calculations and MD simulations have been performed with Jaguar [35] and Desmond [36-39] programs, both as implemented in Schrödinger Materials Science Suite 2015-4. DFT calculations have been performed by B3LYP exchange-correlation functional [40], together with 6-311++G(d,p), 6-31+G(d,p) and 6-311G(d,p) basis sets for the calculations of ALIE, Fukui functions and BDEs, respectively, while MD simulations have been performed with OPLS 2005 force field [41]. Also, in the case of MD simulations, simulation time was set to 10 ns, isothermal–isobaric (NPT) ensemble class was chosen, temperature was set to 300 K, pressure to 1.0325 bar, while cut off radius was set to 12 Å. Simple point charge (SPC) model [42] was used for the theoretical treatment of solvent. System that was investigated by MD

simulations was modeled by placing of one HBAMTT molecule into the cubic box with ~3000 water molecules. Method of Johnson et al. [43,44] was used for the analysis of electron density and determination of intramolecular noncovalent interactions. Maestro GUI [45] was used for the preparation of input files and analysis of results when Schrödinger Materials Science Suite 2015-4 was used. All molecular docking calculations were performed on AutoDock-Vina software [46] and as reported in literature [47]. Amongst the docked conformations, one which binded well at the active site was analyzed for detailed interactions in Discover Studio Visualizer 4.0 software.

4. Results and discussion

In the following discussion, the phenyl and triazole rings are designated as PhI and PhII, respectively.

4.1 Geometrical parameters

The C=S bond length (DFT/XRD) of the title compound is 1.6747/1.6752Å which are in agreement with reported values [14,15]. In the present case, the N-N bond lengths (DFT/XRD) are in the range 1.3761-1.3677/1.3883-1.3693Å, which are in agreement with the literature [48]. The C-C bond lengths in the phenyl ring lie between 1.3827-1.4073Å (DFT) and 1.3784-1.4014Å (XRD) [49]. In the triazole ring, the bond lengths (DFT/XRD) for the C_{10}-N_6, C_{10}-N_5, C_9-N_7 and C_9-N_5 are 1.2981/1.2953, 1.3928/1.3743, 1.3569/1.3343 and 1.4009/1.3923Å, respectively, and in agreement with reported values [14,15]. Also, the C-N bond lengths were intermediate between a C-N single bond (1.47Å) and a C=N double bond (1.22Å) [14], suggesting that some multiple bond character is presented in the molecular system. At C_{18} position, the bond angles (DFT/XRD) are, C_{16}-C_{18}-C_{19} = 120.1/119.8°, C_{16}-C_{18}-O_2 = 122.9/122.3° and C_{19}-C_{18}-O_2 = 117.1/117.8°, and this asymmetry is due to interaction between the oxygen atom and H_{20}. At C_{13}, the bond angles (DFT/XRD), C_{14}-C_{13}-C_{21} = 118.3/118.0°, C_{14}-C_{13}-C_{11} = 118.6/120.1° and C_{21}-C_{13}-C_{11} = 123.0/121.9° and the changes in bond angles are due to the adjacent C=N bond. At N_5 position, the bond angles (DFT/XRD), C_9-N_5-C_{10} and C_{10}-N_5-N_4 are decreased by 1.8/2.0° and 1.8/1.6° while the bond angle, C_9-N_5-N_4 is increased by 13.6/13.6° from 120° which shows interaction between the triazole moiety and neighbouring groups. Similarly at C_9 position, the bond angles (DFT/XRD), N_5-C_9-N_7 = 101.4/102.3°, N_5-C_9-S_1 = 132.6/130.2° and N_7-C_9-S_1 = 125.9/127.5° and this asymmetry in angles is due to the interaction between CS and neighbouring units.

4.2 IR and Raman spectra

Table S3 (supporting material) contains the calculated scaled wavenumber, observed IR, Raman bands and assignments of the title compound.

For the title compound, NH stretching mode is observed at 3388 cm^{-1} (IR) and at 3530 cm^{-1} theoretically with an IR intensity of 100.73 and PED 99% and there is a red shift from computational result which is due to the interaction between NH and CS groups. In the case of different substituted triazole derivatives, the NH stretching modes are reported at 3383 cm^{-1} [50], 3417 cm^{-1} [51] and at 3444 cm^{-1} (IR), 3430 cm^{-1} (Raman) and at 3532 cm^{-1} theoretically [15]. NH group deformation modes are usually in the ranges, 1510-1500, 1450-1250 and 550-430 cm^{-1} [52] and according to literature, if NH is in a closed ring [52, 53] the NH deformation mode is not seen in the region 1510-1500 cm^{-1}. The NH deformation modes of the title compound are assigned at 1450, 480 cm^{-1} (IR), 1449, 480 cm^{-1} (Raman), 1449, 483 cm^{-1} theoretically with high IR intensities, PEDs, 47 and 70%. The reported values of NH deformations of a similar derivative are 1453 and 512 cm^{-1} [15].

The C=N stretching modes of the triazole derivatives are reported at 1597 cm^{-1} [54], 1535-1666 cm^{-1} [55], 1592 cm^{-1} [56] experimentally, at 1584 cm^{-1} theoretically [56] and at 1540 cm^{-1} (IR), 1538 cm^{-1} (Raman), 1533 cm^{-1} (DFT) [15]. The C=N stretching mode of triazole ring of the title compound is observed at 1579 cm^{-1} in the Raman and 1577 cm^{-1} in IR spectrum. The computed value corresponding to this mode is at 1579 cm^{-1} with high IR intensity and Raman activity and a PED of 47%. The CN stretching modes of the triazole ring of the title compound are observed at 1330, 1250 cm^{-1} in the IR spectrum and 1218 cm^{-1} in the Raman spectrum. The corresponding computed values are 1325, 1243 and 1214 cm^{-1} which are in agreement with literature [15] with PEDs, 41, 35 and 42%. The modes at 1325 and 1243 cm^{-1} possess high IR intensities, with low Raman activities, while the mode at 1214 cm^{-1} has a high Raman activity. In the present case, the N-N stretching mode of the triazole ring is assigned at 1082 cm^{-1} and the reported value is at 1080 cm^{-1} [15]. The mode calculated at 1214 cm^{-1} has contributions from C=S stretching and agrees very well with the reported values at 1224-1226 cm^{-1} [57] and at 1228 cm^{-1} [15]. For the title compound, the C11=N4 and N4-N5 stretching modes are assigned at 1601 cm^{-1} and at 987 cm^{-1} theoretically, as expected [58], and the reported values are 1606 and 928 cm^{-1} [14].

In the present case, the CH_3 modes of the title compound are assigned at 2938 cm^{-1} (IR), 3015, 2936 cm^{-1} (Raman), 3024, 2988, 2936 cm^{-1} (DFT) (stretching modes), 1380, 1002, 965 cm^{-1} (IR), 1380, 965 cm^{-1} (Raman), 1436, 1430, 1375, 1000, 967 cm^{-1} (DFT) (deformation modes) as expected [53,59]. For the title compound the OH stretching appears at 3636 cm^{-1}, theoretically as expected in literature [53]. The in-plane OH deformation of the hydroxy group of the title compound assigned at 1393 cm^{-1} theoretically, which is expected in the region 1440 ± 40 cm^{-1} [53]. The C-O stretching band is expected in the region 1220 ± 40 cm^{-1} [58, 59] and this stretching of C-O is observed at 1235 cm^{-1} in the IR spectrum and at 1239 cm^{-1} in Raman spectrum, while the corresponding calculated value is 1240 cm^{-1}. It has moderate IR intensity and Raman activity, has a PED of 39% and is not pure, but contains significant contributions from other modes also. Benzon et al. [60] reported OH in-plane deformation at 1406 cm^{-1} and C-O stretching at 1229 cm^{-1}.

The CH stretching modes of the phenyl ring are observed at 3068, 3031 cm^{-1} in the IR spectrum, 3063, 3035 cm^{-1} in the Raman spectrum and the DFT calculations give these modes as pure modes at 3080, 3065, 3055 and 3030 cm^{-1} with PEDs above 99% for the title compound [53]. The υPhI modes are expected in the region 1280-1630 cm^{-1} for para substituted phenyl rings [53] and the modes observed at 1590, 1498, 1417 cm^{-1} in the IR spectrum, at 1581, 1540, 1494, 1318 cm^{-1} in the Raman spectrum and at 1585, 1555, 1491, 1416, 1321 cm^{-1} theoretically are assigned as υPhI modes. All the phenyl ring stretching modes have PEDs around 44% and all the modes except 1416 cm^{-1} have high IR intensities and the modes at 1585 cm^{-1} and 1555 cm^{-1} have very high Raman activities. For the title compound, the ring breathing mode of the para substituted phenyl ring is confirmed by the band at 848 cm^{-1} in the IR spectrum, 860 cm^{-1} in the Raman spectrum which finds support from computational result at 852 cm^{-1} and the ring breathing mode of the para substituted benzene having different substituent has been expected in the range 780-880 cm^{-1} [61]. The reported value of this mode is at 873 cm^{-1} in the IR spectrum, at 861 cm^{-1} theoretically [62] and at 849 cm^{-1} in the IR spectrum, 852 cm^{-1} theoretically [14]. For the title compound the in-plane and out-of-plane CH modes are observed at 1158, 1130 cm^{-1} (IR), 1280, 1158, 1010 cm^{-1} (Raman) (in-plane deformation) and at 932, 812 cm^{-1} (IR), 818 cm^{-1} (Raman) (out-of-plane deformation). The DFT calculations give these mode at 1282, 1152, 1147, 1087 cm^{-1} (in-plane) and at 937, 897, 815, 778 cm^{-1} (out-of-plane) as expected [53].

4.3 Frontier molecular orbital analysis

The frontier molecular orbital energies and the HOMO-LUMO plot are very useful for predicting the most reactive sites in the molecular system [63] which gives sites of attack of electrophilic and nucleophilic [15]. The HOMO and LUMO energy values for the title compound are -6.988 and -4.826 eV and the energy gap = 2.162 eV which clearly indicates that the charge transfer takes place within the molecule, which increases the molecular activity. The HOMO and LUMO molecular orbitals are shown in Fig. S1 (supporting material) which very clearly gives the charge transfer within the molecule. With respect to the wavefunction in Fig.S1 positive and negative phases of orbtials are colored with green and red colors, respectively. The various chemical descriptors, hardness $\eta = (I-A)/2 = 1.081$ eV, chemical potential $\mu = -(I+A)/2 = -5.907$ eV and global electrophilicity index $\omega = \mu^2/2\eta = 16.14$ eV where $I = -E_{HOMO} = 6.988$ eV and $A = -E_{LUMO} = 4.826$ eV are the first ionization potential and electron affinity [64].

4.4 Molecular electrostatic potential

The molecular electrostatic potential (MEP) plot is used to identify the sites for electrophilic and nucleophilic reactions [15]. The different values of the electrostatic potential are represented by different colours and potential increases in the order of red < orange < yellow < green < blue. In MEP maximum negative region represents the site for electrophilic attack indicated by red color while the maximum positive region represents nucleophilic attack indicated by blue color. As seen from the MEP map (Fig. S2 – supporting material) of the title compound, regions of negative potential are over the electro negative oxygen atoms of the sulfur atom, triazole and phenyl rings and the regions having the positive potential are over the OH and NH hydrogen atoms.

4.5 ALIE surface, Fukui functions and noncovalent interactions

Detection and characterization of molecule sites possibly prone to electrophilic attacks can be efficiently conducted employing the concept of average local ionization energy (ALIE). ALIE was introduced by Sjoberg et al. [65,66] and it has been defined as a sum of orbital energies weighted by the orbital densities according to the following equation:

$$I(r) = \sum_i \frac{\rho_i(\vec{r})|\varepsilon_i|}{\rho(\vec{r})}. \qquad (1)$$

where $\rho_i(\vec{r})$ denotes electronic density of the i-th molecular orbital at the point $\vec{r}$, ε_i denotes orbital energy, while $\rho(\vec{r})$ denotes total electronic density function [67,68]. This quantum molecular descriptor provides the energy necessary to remove electron from some point

around the molecule. The points of interest are the ones where ALIE values are the lowest, since at those locations electrons are the least tightly bonded. The best visualization of ALIE values is by their mapping to the electron density surface, Fig. 4.

Investigation of ALIE surface of title molecule clearly indicates that the most reactive molecule site, from the aspect of electrophilic attacks, is sulfur atom S1. In its near vicinity the ALIE has values of ~158 kcal/mol. On the other side the highest ALIE values are localized in the near vicinity of hydrogen atom H3, belonging to OH group, and in the near vicinity of hydrogen atom H8. These locations are characterized by ALIE values of ~389 kcal/mol. Later it will be shown that these hydrogen atoms have the most pronounced interactions with water molecules, according to RDFs after MD simulations. Fig. 4 also contains one noncovalent interaction, as obtained by analysis of electron density between atoms of HBAMTT molecule. This noncovalent interaction is located between sulfur atom S1 and hydrogen atom H12, with corresponding strength of –0.019 electron/bohr^3.

In the similar manner, by mapping of values to the electron density surface, Fukui functions have been used as well. These functions determine the changes in electron density with the change of charge. In Jaguar program Fukui functions are calculated by finite difference approach according to the following equations:

$$f^{+} = \frac{\left(\rho^{N+\delta}(r) - \rho^{N}(r)\right)}{\delta}, \tag{2}$$

$$f^{-} = \frac{\left(\rho^{N-\delta}(r) - \rho^{N}(r)\right)}{\delta}. \tag{3}$$

where N stands for the number of electrons in reference state of the molecule, while δ stands for the fraction of electron which default value is set to be 0.01 [69]. For the Fukui f^{+} function positive color (purple color in Fig. 5a), determines the molecule sites where electron density increased after the charge addition. On the other side, in the case of Fukui f^{-} function the negative color (red color in Fig. 5b), determines the molecule sites where electron density decreased after the removal of charge. According to the results provided in Fig. 5a, after addition of charge, electron density increases in the near vicinity of carbon atom C11, designating this molecule site as electrophilic. On the other side, in Fig. 5b, the location of red color indicates that, after charge removal, electron density decreases in the near vicinity of benzene ring and in the near vicinity of nitrogen atom N4, designating these molecule sites as nucleophilic.

4.6 Natural Bond Orbital analysis

There strong inter molecular hyper conjugative interactions are N_5-C_9 from S_1 of $n_2(S_1)\rightarrow\sigma^*(N_5\text{-}C_9)$, C_{16}-C_{18} from O_2 of $n_2(O_2)\rightarrow\sigma^*(C_{16}\text{-}C_{18})$, S_1-C_9 from N_5 of $n_1(N_5)\rightarrow\pi^*(S_1\text{-}C_9)$, N7-C9 from N_6 of $n_1(N_6)\rightarrow\sigma^*(N_7\text{-}C_9)$ and S_1-C_9 from N_7 of $n_1(N_7)\rightarrow\pi^*(S_1\text{-}C_9)$. The stabilization energies and electron densities are respectively, 13.77, 28.86, 61.38, 7.46, 74.13 kJ/mol and 0.09370e, 0.38394, 0.58428, 0.06790, 0.58428e. These interactions are observed as an increase in electron density (ED) in C-C, S-C and C-N anti bonding orbitals that weakens the respective bonds.

Also the natural hybrid orbital with low occupation numbers are $n_2(S_1)$ and $n_2(O_2)$ with 100% p-character, higher energies -0.20311 and -0.34523 a.u and low occupation numbers 1.85655 and 1.86756. The orbital with high occupation numbers are $n_1(S_1)$ and $n_1(O_2)$ with lower energies -0.70149 and -0.62471 a.u and p-characters 17.51 and 55.50%) and high occupation numbers, 1.98284 and 1.97966. Thus, a very close to pure p-type lone pair orbital participates in the electron donation to the π*(S-C), π*(N-C) and π*(C-C) orbitals in the compound.

4.7 Nonlinear optical properties

NLO properties like the dipole moment, polarizability, first and second order hyperpolarizabilites are calculated using B3LYP/6-311++G(d) (5D, 7F). The total molecular dipole moment of the title compound is 3.1132 Debye, polarizability is 2.856×10^{-23} esu, and the first and second order hyperpolarizabilities are 10.446×10^{-30} and -12.00×10^{-37} esu. The first hyperpolarizability of the title compound is 80.35 times that of the standard NLO material, urea [70] and the reported values of similar derivatives are 2.43×10^{-30} [15] and 26.879×10^{-30} [14]. The larger component of second order hyperpolarizability is associated with the larger ground state polarization which leads to strong electronic coupling between the ground and the low lying excited states. Also, the NLO properties are related to the energy gap between HOMO and LUMO. The energy gap of the title compound is 2.162 eV which is lower than that of urea (6.7 eV) [70]. Therefore, the investigated molecule could be suitable for nonlinear optical applications.

4.8 Reactive and degradation properties based on autoxidation and hydrolysis

In order to improve interpretation of forced degradation studies it is very useful to perform DFT calculations and MD simulations, in order to gain an insight into the reactive properties which principally determine degradation mechanisms [71-74]. For these purposes it is

especially useful to calculate BDE for hydrogen abstraction, in order to predict possibilities for autoxidation mechanism, and RDFs, in order to predict possibilities for hydrolysis mechanism. If the BDE values for hydrogen abstraction are within certain range, than target molecule can be vulnerable towards autoxidation mechanism and the particular location of that hydrogen molecule is important reactive center. According to the study of Wright et al. [75] pharmaceutical molecule is the most sensitive towards autoxidation mechanism if the BDE ranges from 70 to 85 kcal/mol, while BDE lower than 70 kcal/mol are not suitable for autoxidation mechanism, due to the resistance of formed radicals for the O_2 insertion [26, 76, 77]. However, Gryn'ova [78] states that BDE values for hydrogen abstraction between 85 kcal/mol to 90 kcal/mol are questionable, but still in the race for autoxidation mechanism. BDE values for hydrogen abstraction together with BDE for the rest of the single acyclic bonds are provided in Fig. 6.

According to the calculated BDE values, Fig. 6, it can be seen that there is one O-H bond (denoted with number 1) with corresponding BDE value of ~89 kcal/mol, which could be interesting for the sensitivity of title molecule towards the autoxidation mechanism. All other BDE values for hydrogen abstraction are much higher than the upper limit of 90 kcal/mol. On the other side, BDE values for the rest of the single acyclic bonds have also been presented in Fig. 6 and the lowest has been calculated for the bond denoted with number 8, with the BDE value of just ~54 kcal/mol. These two molecule sites are important and degradation process could start precisely at them. It is also important to note that nitrogen atom N4, involved in the lowest BDE bond, is also recognized as important reactive center according to the Fukui functions.

HBAMTT molecule also has interesting interactions with water molecules, according to calculated RDFs after MD simulation. RDF, g(*r*), indicates the probability of finding a particle in the distance *r* from another particle [79] and in this study it has been shown that total of seven atoms of HBAMTT molecule have pronounced interactions with water molecules, Fig. 7.

Seven atoms with pronounced interactions are nitrogen atom N6, carbon atoms C10 and C23, sulfur atom S1, oxygen atom O2 and, the most important, hydrogen atoms H3 and H8. Aforementioned carbon atoms have similar g(r) curves in terms of peak distance, which is located at around 3.5 Å, while maximal g(r) value is somewhat higher in the case of C23 atom (1.35 comparing to 1.15). Nitrogen atom N6 has peak distance located at much higher distance

than carbon atoms, at around 4.7 Å and its maximal g(r) value is around 1.3. According to RDFs it can be stated that much more pronounced interactions with water molecules occur in the case of oxygen, sulfur and hydrogen molecules. Sulfur atom S1 has peak distance located at around 3.7 Å with maximal g(r) value of around 1.3, while oxygen atom O2 has peak distance located at around 2.6 Å with the highest of all maximal g(r) values (somewhat higher than 1.4). Two hydrogen atoms have peak distances located significantly under 2 Å, with H3 having much higher maximal g(r) value than H8 (~1.4 comparing to ~0.9), indicating the strongest interactions with water molecules. In the same time in Fig. 7 two distinct solvation spheres can be seen in the case of H3. Significant interactions of hydrogen atom H3 also indicate that hydrolysis mechanism could compete with autoxidation mechanism at the same location, since the lowest BDE for hydrogen abstraction was calculated for precisely hydrogen atom H3.

4.9 Molecular docking

Medicinally the acetylcholinesterase (AChE) has been targeted in treatments for Alzheimer's disease, myasthenia gravis, and glaucoma, and in the recovery of victims of nerve agent exposure. Agrochemically, AChE is the most widely exploited insecticide target: all the commercial organophosphate and carbamate agents are believed to exert their effects through irreversible inhibition of the enzyme. High resolution crystal structure of protein target were downloaded from the protein data bank website (PDB ID: 1HBJ) [80]. The predicted conformation result was same with crystal structure in reliable RMSD values of 2Å [81]. The ligand binds at the active site of the substrate (Figs. S3 and S4 – supporting material) by conventional hydrogen bonds and pi-amide stacking interactions. Amino acids PHE288 and ARG289 form H-bonds with sulphur atom. LEU282 and ILE287 form pi-sigma interactions with the benzene ring and triazole ring. The docked ligand title compound forms a stable complex with AChE and gives a binding affinity (ΔG in kcal/mol) value of -10.9 (table 2). The title compound shows the inhibitory activity against substrate and can be developed as a new drug for the Alzheimer’s disease, myasthenia gravis and glaucoma.

5. Conclusion

4-[(*E*)-(4-hydroxybenzylidene)amino]-3-methyl-1*H*-1,2,4-triazole-5(4*H*)-thione was synthesized and characterized by theoretical and experimental methods using B3LYP/6-311++G(d) (5D, 7F) level of theory. Wavenumbers, molecular structure, MEP, NBO and NLO analysis were carried out. The geometrical parameters provided by DFT level are in agreement with the XRD data.

Regions of negative potential are over the electro negative oxygen atoms of the sulfur atom, triazole and phenyl rings and the regions having the positive potential are over the OH and NH hydrogen atoms. The first hyperpolarizability of the title compound is 80.35 times that of the standard NLO material urea. DFT calculations of ALIE values and their subsequent mapping to the electron density surface recognized sulfur atom S1 as the most important molecular site from the aspect of electrophilic attacks, with ALIE value of ~158 kcal/mol. Besides sulfur atom, according to the Fukui functions, carbon atom C11 and nitrogen atom N4 have also been recognized as possibly important reactive centers. BDE values for hydrogen abstraction indicate one location possibly prone to autoxidation mechanism. That is hydrogen atom H3 which also has the most pronounced interactions with water molecules, according to RDFs, which decreases the possibility for autoxidation mechanisms due to the competition with hydrolysis mechanism. Other most important RDFs have been calculated for hydrogen atom H8 and for oxygen atom O2.From the docking studies, amino acids PHE288 and ARG289 form H-bonds with sulphur atom and LEU282 and ILE287 form pi-sigma interactions with the benzene ring and triazole ring.

Acknowledgments

The authors would like to extend their sincere appreciation to the Deanship of Scientific Research at King Saud University for funding this work through the Research Group Project No. RG-1436-024. Part of this work has been performed thanks to the support received from Schrödinger Inc.

References

[1] N. Galic, B. Peric, B. Kojic-Prodic, Z. Cimerman, Structural and spectroscopic characteristics of aroylhydrazones derived from nicotinic acid hydrazide, J. Med. Chem. 559 (2001) 187-194.

[2] E. Wyrzykiewicz, D. Purkah, New isomeric N-substituted hydrazones of 2,3- and 4-pyridinecarboxaldehydes, J. Heterocycl. Chem. 35 (1998) 381-387.

[3] A. Dornow, H.Menzel, P. Marx, Syntheses of nitrogen containing heterocycles. XXVII. 1,2,4-triazines. 1. Preparation of some new s-triazolo[3,2-c]-12-triazines, Chem. Ber. 97 (1964) 2173-2178.

[4] A.M. Alafeefy, M.A. Bakht, M.A. Ganaie, M.N. Ansarie, N.N. El-Sayed, A.S.Awaad, Synthesis, analgesic, anti-inflammatory and anti-ulcerogenic activities of certain novel Schiff's bases as fenamate isoesters, Bioorg. Med. Chem. Lett. 25 (2015) 179-183.

[5] H. Barrera, J.M. Vinas, M. Font-Altaba, X. Solans, Synthesis, crystal structure and spectroscopic characterization of af-dichloro-bd,ec-bis{m-[2-(1-methyl-2-piperidinyl)ethanethiolato]-S,N.,m.u.-S}dipalladium(II), Polyhedron 4 (1985) 2027-2030.

[6] S. Malik, S. Ghosh, L. Mitu, Complexes of some 3d-metals with a Schiff base derived from 5-acetamido-1,3,4-thiadiazole—2sulphonamide and their biological activity, J. Serb. Chem. Soc. 76 (2011) 1387-1394.

[7] D.S. Schiller, H.B. Fung, Posaconazole, an extended spectrum triazole antifungal agent, Clin. Ther. 29 (2007) 1862-1886.

[8] R. Herbrecht, D. Denning, T. Patterson, J. Bennett, R. Greene, J. Oestmann, W. Kern, K. Marry, P. Ribaud, O. Lortholary, R. Sylvester, R. Rubin, J. Wingard, P. Starki, C. Durand, D. Caillot, E. Thiel, P. Chandrasekar, M. Hodges, H. Schlamm, P. Troke, B. de Pauw, Voriconazole versus amphotericin B for primary therapy of invasive aspergillosis, N. Engl. J. Med. 347(V) (2002) 408-415.

[9] J. Xu, Y. Cao, J. Zhang, S. Yu, Y. Zou, X. Chai, Q. Wu, D. Zhang, Y. Jiang, Q. Sun, Design, synthesis and antifungal activities of novel 1,2,4-triazole derivatives, Eur. J. Med. Chem. 46 (2011) 3142-3148.

[10] G.L. Almajan, S.F. Barbuceanu, E. Almajan, C. Draghici, G. Saramet, Synthesis, characterization and antibacterial activity of some triazole Mannich bases carrying diphenylsulfone moieties, Eur. J. Med. Chem. 44 (2009) 3083-3089.

[11] P.C. Wade, B.R. Vogt, T.P. Kissick, L.M. Simpkins, D.M. Palmers, R.C. Millonig, 1-acyltriazoles as anti-inflammatory agents, J. Med. Chem. 25 (1982) 331-333.

[12] B. Tozkoparan, E. Kupeli, E. Yesilada, M. Ertan, Preparation of 5-aryl-3-alkylthio-1,2,4-triazoles and corresponding solfones with anti-inflammatory-analgesic activity, Bioorg. Med. Chem. 15 (2007) 1808-1814.

[13] L. Navidpour, H. Shafaroodi, K. Abdi, M. Amini, M.H. Ghahremani, A.R. Dehpour, A. Shafiee, Design, synthesis and biological evaluation of substituted 3-alkylthio-4,5-diaryl-4H-1,2,4-triazoles as selective COX-2 inhibitors, Bioorg. Med. Chem. 14 (2006) 2507-2517.

[14] C.Y. Panicker, H.T. Varghese, P.S. Manjula, B.K. Sarojini, B. Narayana, J.A. War, S.K. Srivastava, C. Van Alsenoy, A.A. Al-Saadi, FT-IR, HOMO-LUMO, NBO, MEP analysis and molecular docking study of 3-methyl-4-{(4-(methylsulfanyl)-benzylidene]amino}-1H-1,2,4-triazole-5(4H)-thione, Spectrochim. Acta A 151 (2015) 198-207.

[15] S.H.R. Sebastian, M.I. Attia, M.S. Almutairi, A.A. El-Emam, C.Y. Panicker, C. Van Alsenoy, FT-IR, FT-Raman, molecular structure, first order hyperpolarizability, HOMO and LUMO analysis, MEP and NBO analysis of 3-(adamantan-1-yl)-4-(prop-2-en-1-yl)-1H-1,2,4-triazole-5(4H)-thione, a potential bioactive agent, Spectrochim. Acta 132 (2014) 295-304.

[16] S. Armaković, S.J. Armaković, J.P. Šetrajčić, I.J. Šetrajčić, Active components of frequently used β-blockers from the aspect of computational study, J. Mol. Model. 18 (2012) 4491-4501.

[17] B. Abramović, S. Kler, D. Šojić, M. Laušević, T. Radović, D. Vione, Photocatalytic degradation of metoprolol tartrate in suspensions of two TiO 2-based photocatalysts with different surface area. Identification of intermediates and proposal of degradation pathways, J. Hazard. Mater. 198 (2011) 123-132.

[18] S.J. Armaković, S. Armaković, N.L. Finčur, F. Šibul, D. Vione, J.P. Šetrajčić, and B. Abramović, Influence of electron acceptors on the kinetics of metoprolol photocatalytic degradation in TiO 2 suspension. A combined experimental and theoretical study, RSC Advances, 5 (2015) 54589-54604.

[19] M. Blessy, R.D. Patel, P.N. Prajapati, Y. Agrawal, Development of forced degradation and stability indicating studies of drugs—A review, J. Pharm. Anal. 4 (2014) 159-165.

[20] J.J. Molnar, J. Agbaba, B. Dalmacija, M. Klašnja, M. Watson, M. Kragulj, Effects of ozonation and catalytic ozonation on the removal of natural organic matter from groundwater, J. Environ. Engineering, 138 (2011) 804-808.

[21] J.J. Molnar, J.R. Agbaba, B.D. Dalmacija, M.T. Klašnja, M.B. Dalmacija, M.M. Kragulj, A comparative study of the effects of ozonation and TiO 2-catalyzed ozonation on the selected chlorine disinfection by-product precursor content and structure, Sci. Total Environ. 425 (2012) 169-175.

[22] D.V. Šojić, D.Z. Orčić, D.D. Četojević-Simin, N.D. Banić, B.F. Abramović, Efficient removal of sulcotrione and its formulated compound Tangenta® in aqueous TiO 2

suspension: Stability, photoproducts assessment and toxicity, Chemosphere, 138 (2015) 988-994.

[23] D.V. Šojić, D.Z. Orčić, D.D. Četojević-Simin, V.N. Despotović, B.F. Abramović, Kinetics and the mechanism of the photocatalytic degradation of mesotrione in aqueous suspension and toxicity of its degradation mixtures, J. Mol. Catalysis A: Chemical, 392 (2014) 67-75.

[24] D.D. Četojević-Simin, S.J. Armaković, D.V. Šojić, B.F. Abramović, Toxicity assessment of metoprolol and its photodegradation mixtures obtained by using different type of TiO 2 catalysts in the mammalian cell lines, Sci. Total Environ. 463 (2013) 968-974.

[25] P. Lienard, J. Gavartin, G. Boccardi, M. Meunier, Predicting drug substances autoxidation, Pharm. Res. 32 (2015) 300-310.

[26] G.L. de Souza, L.M. de Oliveira, R.G. Vicari, A. Brown, A DFT investigation on the structural and antioxidant properties of new isolated interglycosidic O-(1→ 3) linkage flavonols, J. Mol. Model. 22 (2016) 1-9.

[27] Z. Sroka, B. Żbikowska, J. Hładyszowski, The antiradical activity of some selected flavones and flavonols, Experimental and quantum mechanical study, J. Mol. Model. 21 (2015) 1-11.

[28] H. Djeradi, A. Rahmouni, and A. Cheriti, Antioxidant activity of flavonoids: a QSAR modeling using Fukui indices descriptors, J. Mol. Model. 20 (2014) 1-9.

[29] B.K. Sarojini, P.S. Manjula, B. Narayana, J.P. Jasinski, 4-[(E)-(4-hydroxybenzylidene)amino]-3-methyl-1H-1,2,4-triazole-5(4H)-thione, Acta Cryst. E70 (2014) o733-o734.

[30] Gaussian 09, Revision B.01, M.J. Frisch, G.W. Trucks, H.B. Schlegel, G.E. Scuseria, M.A. Robb, J.R. Cheeseman, G. Scalmani, V. Barone, B. Mennucci, G.A. Petersson, H. Nakatsuji, M. Caricato, X. Li, H.P. Hratchian, A.F. Izmaylov, J. Bloino, G. Zheng, J.L. Sonnenberg, M. Hada, M. Ehara, K. Toyota, R. Fukuda, J. Hasegawa, M. Ishida, T. Nakajima, Y. Honda, O. Kitao, H. Nakai, T. Vreven, J.A. Montgomery, Jr., J.E. Peralta, F. Ogliaro, M. Bearpark, J.J. Heyd, E. Brothers, K.N. Kudin, V.N. Staroverov, T. Keith, R. Kobayashi, J. Normand, K. Raghavachari, A. Rendell, J.C. Burant, S.S. Iyengar, J. Tomasi, M. Cossi, N. Rega, J.M. Millam, M. Klene, J.E. Knox, J.B. Cross, V. Bakken, C. Adamo, J. Jaramillo, R. Gomperts, R.E. Stratmann, O. Yazyev, A.J. Austin, R. Cammi,

C. Pomelli, J.W. Ochterski, R.L. Martin, K. Morokuma, V.G. Zakrzewski, G.A. Voth, P. Salvador, J.J. Dannenberg, S. Dapprich, A.D. Daniels, O. Farkas, J.B. Foresman, J.V. Ortiz, J. Cioslowski, D.J. Fox, Gaussian, Inc., Wallingford CT, 2010.

[31] J.B. Foresman, in: E. Frisch (Ed.), Exploring Chemistry with Electronic Structure Methods: A Guide to Using Gaussian, Pittsburg, PA, 1996.

[32] R. Dennington, T. Keith, J. Millam, Gaussview, Version 5, Semichem Inc., ShawneeMission KS, 2009.

[33] J.M.L. Martin, C. Van Alsenoy, GAR2PED, A Program to Obtain a Potential Energy Distribution from a Gaussian Archive Record, University of Antwerp, Belgium, 2007.

[34] E.D. Glendening, A.E. Reed, J.E. Carpenter, F. Weinhold, NBO Version 3.1, Gaussian Inc., Pittsburgh, PA.

[35] A.D. Bochevarov, E. Harder, T.F. Hughes, J.R. Greenwood, D.A. Braden, D.M. Philipp, D. Rinaldo, M.D. Halls, J. Zhang, R.A. Friesner, Jaguar: A high-performance quantum chemistry software program with strengths in life and materials sciences, Int. J. Quantum Chem. 113(18) (2013) 2110-2142.

[36] D. Shivakumar, J. Williams, Y. Wu, W. Damm, J. Shelley, W. Sherman, Prediction of absolute solvation free energies using molecular dynamics free energy perturbation and the OPLS force field, J. Chem. Theory Comput. 6 (2010) 1509-1519.

[37] Z. Guo, U. Mohanty, J. Noehre, T.K. Sawyer, W. Sherman, G. Krilov, Probing the α-Helical Structural Stability of Stapled p53 Peptides: Molecular Dynamics Simulations and Analysis, Chem. Biol. Drug Design, 75 (2010) 348-359.

[38] K.J. Bowers, E. Chow, H. Xu, R.O. Dror, M.P. Eastwood, B.A. Gregersen, J.L. Klepeis, I. Kolossvary, M.A. Moraes, F.D. Sacerdoti. *Scalable algorithms for molecular dynamics simulations on commodity clusters*. in *SC 2006 Conference, Proceedings of the ACM/IEEE*. 2006. IEEE.

[39] I. Fabijanić, C.J. Brala, V. Pilepić, The DFT local reactivity descriptors of α-tocopherol, J. Mol. Model. 21 (2015) 1-7.

[40] A.D. Becke, Density-functional thermochemistry. III. The role of exact exchange, J. Chem. Phys. 98 (1993) 5648-5652.

[41] J.L. Banks, H.S. Beard, Y. Cao, A.E. Cho, W. Damm, R. Farid, A.K. Felts, T.A. Halgren, D.T. Mainz, J.R. Maple, Integrated modeling program, applied chemical theory (IMPACT), J. Comput. Chem. 26 (2005) 1752-1780.

[42] H.J. Berendsen, J.P. Postma, W.F. van Gunsteren, J. Hermans, *Interaction models for water in relation to protein hydration*, in *Intermolecular forces*. 1981, Springer. p. 331-342.

[43] A. Otero-de-la-Roza, E.R. Johnson, J. Contreras-García, Revealing non-covalent interactions in solids: NCI plots revisited, Phys. Chem. Chem. Phys. 14 (2012) 12165-12172.

[44] E.R. Johnson, S. Keinan, P. Mori-Sanchez, J. Contreras-Garcia, A.J. Cohen, W. Yang, Revealing noncovalent interactions, J. Am. Chem. Soc. 132 (2010) 6498-6506.

[45] *Schrödinger Release 2015-4: Maestro, version 10.4, Schrödinger, LLC, New York, NY*, 2015.

[46] O. Trott, A.J. Olson, AutoDock Vina: Improving the speed and accuracy of docking with a new scoring function, efficient optimization and multithreading, J. Comput. Chem. 31 (2010) 455-461.

[47] R.I. Al-Wabli, K.S. Resmi, Y.S. Mary, C.Y. Panicker, M.A. Attia, A.A. El-Emam, C. Van Alsenoy, Vibrational spectroscopic studies, Fukui functions, HOMO-LUMO, NLO, NBO analysis and molecular docking study of (E)-1-(1,3-benzodioxol-5-yl)-4,4-dimethylpent-1-en-3-one, a potential precursor to bioactive agents, J. Mol. Struct. 1123 (2016) 375-383.

[48] P.S. Binil, Y.S. Mary, H.T. Varghese, C.Y. Panicker, M.R. Anoop, T.K. Manojkumar, Infrared and Raman spectroscopic analyses and theoretical computation of 4-butyl-1-(4-hydroxyphenyl)-2-phenyl-3,5-pyrazolidinedione, Spectrochim. Acta 94 (2012) 101-109.

[49] Y.S. Mary, K. Raju, I. Yildiz, O. Temiz-Arpaci, H.I.S. Nogueira, C.M. Granadeiro, C. Van Alsenoy, FT-IR, FT-Raman, SERS and computational study of 5-ethylsulphonyl-2-(o-chlorobenzyl)benzoxazole, Spectrochim. Acta 96 (2012) 617-625.

[50] R. Ustabas, N. Suleymanoglu, H. Tanak, Y.B. Alpaslan, Y. Unveer, K. Sancak, Experimental and theoretical studies of the molecular structure o f4-(3-(1H-imidazol-1-yl)propyl)-5-p-toltyl-2H-1,2,4-triazol-3(4H)-one, J. Mol. Struct. 984 (2010) 137-145.

[51] K. Sancak, Y. Unver, H. Tanak, I. Degirmenciouglu, E. Dugdu, M. Er, S.Isik, Thesynthesis of some new imidazole and triazole derivatives: crystal structure and DFT-

TDDFT investigation on electronic structure, J. Inclusion Phenom. Macrocyclic Chem. 67 (2010) 325-334.

[52] G. Socrates, Infrared Characteristic Group Frequencies, John Wiley and Sons, New York, 1981.

[53] N.P.G. Roeges, A Guide to the Complete Interpretation of IR Spectra of Organic Compounds, Wiley, New York, 1994.

[54] O. Bekircan, H. Bektas, Synthesis of new bis-1,2,4-triazole derivatives, Molecules 11 (2006) 469-477.

[55] S. Genc, N. Dege, A. Cetin, A. Cansiz, M. Sekerci, M. Dincer, 3-(2-hydroxyphenyl)-4-phenyl-1H-1,2,4-triazole-5(4H)-thione, Acta Cryst. E60 (2004) o1580-o1582.

[56] H. Tanak, Y. Koysal, Y. Onver, M. Yavuz, S. Isik, K. Sancak, An experimental and DFT computational study on 4-(3-(1H-imidazol-1-yl)propyl)-5-methyl-2H-1,2,4-triazol-4(4H)-one monohydrate, Mol. Phys. 108 (2010) 127-139.

[57] O.D. Cretu, S.F. Barbuceanu, G. Saramet, C. Draghici, Synthesis and characterization of some 1,2,4-triazole-3-thiones obtained from intramolecular cyclization of new 1-(4-(4-X-phenylsulfonyl)benzoyl)-4-(4-iodophenyl)-3-thiosemicarbazides, J. Serb. Chem. Soc. 75 (2010) 1463-1472.

[58] R.M. Silverstein, G.C. Bassler, T.C. Morril, Spectrometric Identification of Organic Compounds, fifth ed., John Wiley and Sons Inc., Singapore, 1991.

[59] N.B. Colthup, L.H. Daly, S.E. Wiberly, Introduction of Infrared and Raman Spectroscopy, Academic Press, New York, 1975.

[60] K.B. Benzon, H.T. Varghese, C.Y. Panicker, K. Pradhan, B.K. Tiwary, A.K. Nanda, C.Van Alsenoy, Spectroscopic investigation (FT-IR and FT-Raman), vibrational assignments, HOMO-LUMO, NBO, MEP analysis and molecular docking study of 2-(4-hyroxyphenyl)-4,5-dimethyl-1H-imidazole-3-oxide, Spectrochim. Acta 146 (2015) 307-322.

[61] G. Varsanyi, Assignments of Vibrational Spectra of Seven Hundred Benzene Derivatives, Wiley, New York, 1974.

[62] C.Y. Panicker, K.R. Ambujakshan, H.T. Varghese, S. Mathew, S. Ganguli, A.K. Nanda, C. Van Alsenoy, FT-IR, FT-Raman and DFT calculations of 3-{[(4-

fluorophenyl)methylene]amino}-2-phenylquinazolin-4(3H)-one, J. Raman Spectrosc. 40 (2009) 527-536.

[63] K. Fukui, T. Yonezawa, H. Shingu, A molecular orbital theory of reactivity in aromatic hydrocarbons, J. Chem. Phys. 20 (1952) 722-725.

[64] R.J. Parr, R.G. Pearson, Absolute hardness, companion parameter to absolute electronegativity, J. Am. Chem. Soc. 105 (1983) 7512-7516

[65] J.S. Murray, J.M. Seminario, P. Politzer, Sjoberg, Average local ionization energies computed on the surfaces of some strained molecules, Int. J. Quantum Chem. 38 (1990) 645-653.

[66] P. Politzer, F. Abu-Awwad, J.S. Murray, Comparison of density functional and Hartree–Fock average local ionization energies on molecular surfaces, Int. J. Quantum Chem. 69 (1998) 607-613.

[67] F.A. Bulat, A. Toro-Labbé, T. Brinck, J.S. Murray, P. Politzer, Quantitative analysis of molecular surfaces: areas, volumes, electrostatic potentials and average local ionization energies, J. Mol. Model. 16 (2010) 1679-1691.

[68] P. Politzer, J.S. Murray, F.A. Bulat, Average local ionization energy: a review, J. Mol. Model. 16 (2010) 1731-1742.

[69] A. Michalak, F. De Proft, P. Geerlings, R. Nalewajski, Fukui functions from the relaxed Kohn-Sham orbitals, J. Phys. Chem. A 103 (1999) 762-771.

[70] C. Adant, M. Dupuis, J.L. Bredas, Ab initio study of the nonlinear optical properties of urea, electron correlation and dispersion effects, Int. J. Quantum Chem. 56 (1995) 497-507.

[71] X. Ren, Y. Sun, X. Fu, L. Zhu, Z. Cui, DFT comparison of the OH-initiated degradation mechanisms for five chlorophenoxy herbicides, J. Mol. Model. 19 (2013) 2249-2263.

[72] L.-l. Ai, J.-y. Liu, Mechanism of OH-initiated atmospheric oxidation of E/Z-CF3CF= CFCF3: a quantum mechanical study, J. mol. Model. 20 (2014) 1-10.

[73] W. Sang-aroon, V. Amornkitbamrung, V. Ruangpornvisuti, A density functional theory study on peptide bond cleavage at aspartic residues: direct vs cyclic intermediate hydrolysis, J. Mol. Model. 19 (2013) 5501-5513.

[74] J. Kieffer, É. Brémond, P. Lienard, G. Boccardi, In silico assessment of drug substances chemical stability, J. Mol. Struct. THEOCHEM, 954 (2010) 75-79.

[75] J.S. Wright, H. Shadnia, L.L. Chepelev, Stability of carbon-centered radicals: Effect of functional groups on the energetics of addition of molecular oxygen, J. Comput. Chem. 30 (2009) 1016-1026.

[76] J.S. Wright, H. Shadnia, L.L. Chepelev, Stability of carbon-centered radicals: Effect of functional groups on the energetics of addition of molecular oxygen, J. Comput. Chem. 30 (2009) 1016-1026.

[77] T. Andersson, A. Broo, E. Evertsson, Prediction of Drug Candidates' Sensitivity Toward Autoxidation: Computational Estimation of C-H Dissociation Energies of Carbon-Centered Radicals, J. Pharm. Sci. 103 (2014) 1949-1955.

[78] G. Gryn'ova, J.L. Hodgson, M.L. Coote, Revising the mechanism of polymer autoxidation, Org. Biomol. Chem. 9 (2011) 480-490.

[79] R.V. Vaz, J.R. Gomes, C.M. Silva, Molecular dynamics simulation of diffusion coefficients and structural properties of ketones in supercritical CO_2 at infinite dilution, J. Supercritic. Fluids, 107 (2016) 630-638.

[80] C. Doucet-Personeni, P.D. Bentley, R.J. Fletcher, A. Kinkaid, G. Kryger, B. Pirard, A. Taylor, J. Taylor, R. Viner, I. Silman, J.L. Sussman, H.M. Greenblat, T.L. Lewis, A structure based design approach to the development of novel, reversible AChE inhibitors, J. Med. Chem. 44 (2001) 3203-3215.

[81] B. Kramer, M. Rarey, T. Lengauer, Evaluation of the FlexX incremental construction algorithm for protein ligand docking, PROTEINS: Struct. Funct. Genet. 37 (1999) 228-241.

Figure Captions

Fig. 1 FT-IR spectrum of 4-[(*E*)-(4-hydroxybenzylidene)amino]-3-methyl-1*H*-1,2,4-triazole-5(4*H*)-thione

Fig. 2 FT-Raman spectrum of 4-[(*E*)-(4-hydroxybenzylidene)amino]-3-methyl-1*H*-1,2,4-triazole-5(4*H*)-thione

Fig. 3 Optimized geometry of 4-[(*E*)-(4-hydroxybenzylidene)amino]-3-methyl-1*H*-1,2,4-triazole-5(4*H*)-thione

Fig. 4 ALIE surface of 4-[(*E*)-(4-hydroxybenzylidene)amino]-3-methyl-1*H*-1,2,4-triazole-5(4*H*)-thione molecule

Table 1

Second-order perturbation theory analysis of Fock matrix in NBO basis corresponding to the intramolecular bonds of the title compound

Donor(i)	type	ED/e	Acceptor(j)	Type	ED/e	E(2)[a]	E(j)-E(i)[b]	F(i,j)[c]
S1-C9	σ	1.98194	N6-N7	σ*	0.02080	2.49	1.06	0.046
S1-C9	π	1.98128	S1-C9	π*	0.58428	5.79	0.21	0.036
N4-C11	σ	1.98722	N5-C10	σ*	0.04952	2.20	1.30	0.048
N4-C11	π	1.92979	C13-C14	π*	0.38764	7.52	0.37	0.051
N5-C9	σ	1.98267	C10-C23	σ*	0.01573	2.94	1.24	0.054
N5-C10	σ	1.98060	S1-C9	σ*	0.01045	4.37	1.11	0.062
-	σ	1.98060	N4-C11	σ*	0.00883	2.18	1.42	0.050
N6-C10	σ	1.98441	N4-N5	σ*	0.03063	2.87	1.23	0.053
-	σ	1.98441	C10-C23	σ*	0.01573	2.13	1.30	0.047
N7-C9	σ	1.98813	N4-N5	σ*	0.03063	4.91	1.21	0.069
C16-C18	σ	1.97878	C14-C16	σ*	0.01314	2.97	1.29	0.055
-	σ	1.97878	C18-C19	σ*	0.02518	4.02	1.27	0.064
C16-C18	π	1.64584	C13-C14	π*	0.38764	23.67	0.29	0.075
-	π	1.64584	C19-C21	π*	0.27757	14.55	0.30	0.060
LPS1	σ	1.98284	N5-C9	σ*	0.09370	4.66	1.06	0.064
LPS1	π	1.85665	N5-C9	σ*	0.09370	13.77	0.56	0.079
-	π	1.85665	N7-C9	σ*	0.06790	11.71	0.63	0.078
LPO2	σ	1.97966	C16-C18	σ*	0.02707	6.06	1.17	0.075
LPO2	π	1.86756	C16-C18	π*	0.38394	28.86	0.35	0.095
LPN4	σ	1.92688	N5-C9	σ*	0.09370	11.86	0.76	0.085
LPN5	σ	1.55964	S1-C9	π*	0.58428	61.38	0.22	0.107
-	σ	1.55964	N4-C11	π*	0.19358	21.83	0.30	0.077
-	σ	1.55964	N6-C10	π*	0.29472	40.31	0.29	0.100
LPN6	σ	1.93955	N5-C10	σ*	0.04952	6.11	0.82	0.064
-	σ	1.93955	N7-C9	σ*	0.06790	7.46	0.86	0.072
LPN7	σ	1.60100	S1-C9	π*	0.58428	74.13	0.21	0.117
-	σ	1.60100	N6-C10	π*	0.29472	23.89	0.28	0.075

[a]E(2) means energy of hyper-conjugative interactions (stabilization energy in kJ/mol)

[b]Energy difference (a.u.) between donor and acceptor i and j NBO orbitals

[c]F(i,j) is the Fock matrix elements (a.u.) between i and j NBO orbitals

Table 2

Binding affinity of different poses of the title compound as predicted by Autodock Vina.

Mode	Affinity	Distance from best mode	
-	(kcal/mol)	RMSD 1.b.	RMSD u.b.
1	-10.9	0.000	0.000
2	-10.2	2.008	8.346
3	-9.3	2.373	4.794
4	-9.3	2.236	5.186
5	-8.6	2.376	3.548
6	-8.4	12.047	14.496
7	-8.1	4.790	8.273
8	-7.6	2.719	9.762
9	-7.5	3.384	8.217

In One figure green dotted line corresponds to conventional hydrogen bond and violet dotted lines represents pi-sigma interactions.

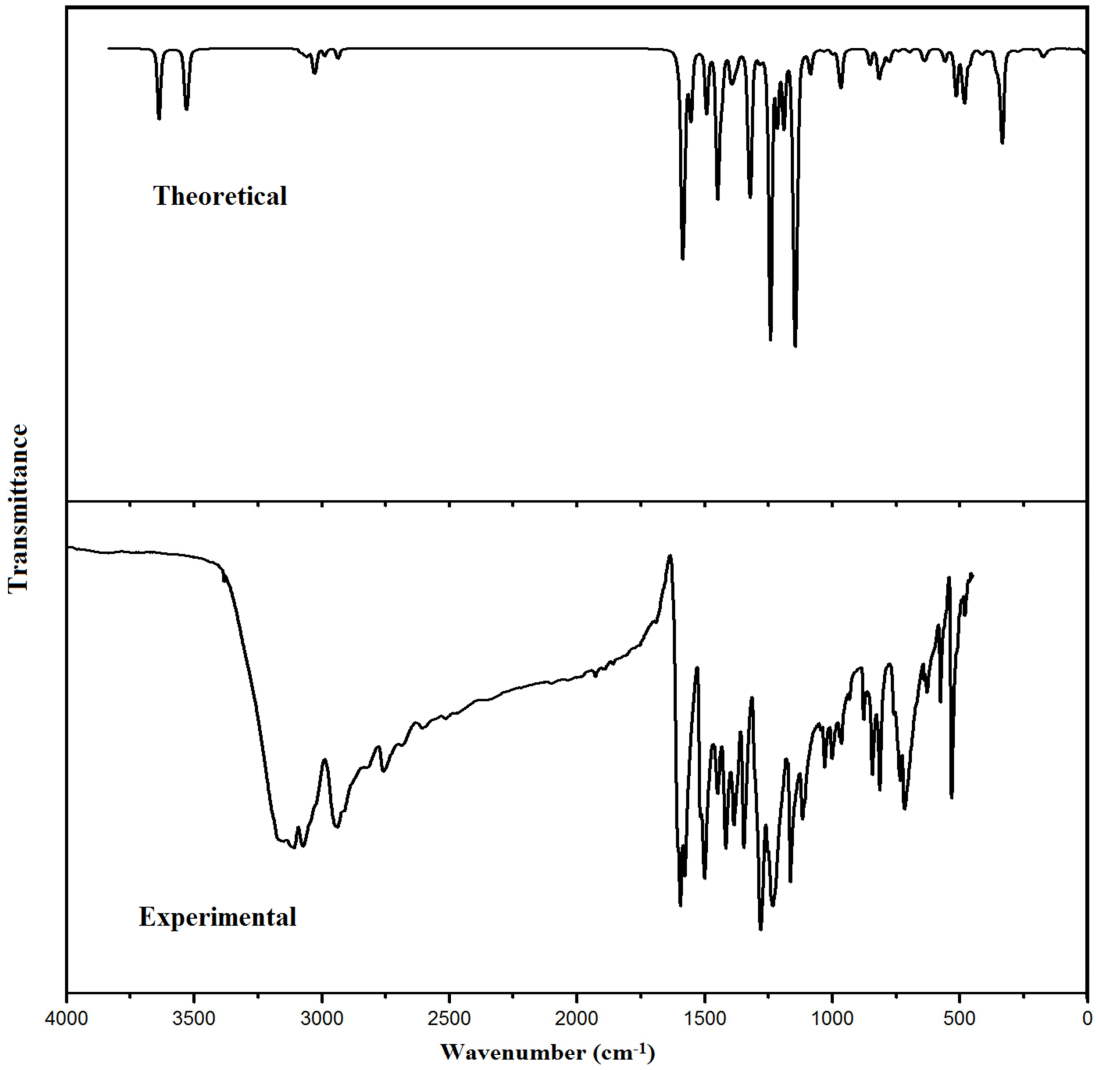

Fig.1 F-IR spectrum of 4-[(E)-(4-hydroxybenzylidene)amino]-3-methyl-1H-1,2,4-triazole-5(4H)-thione

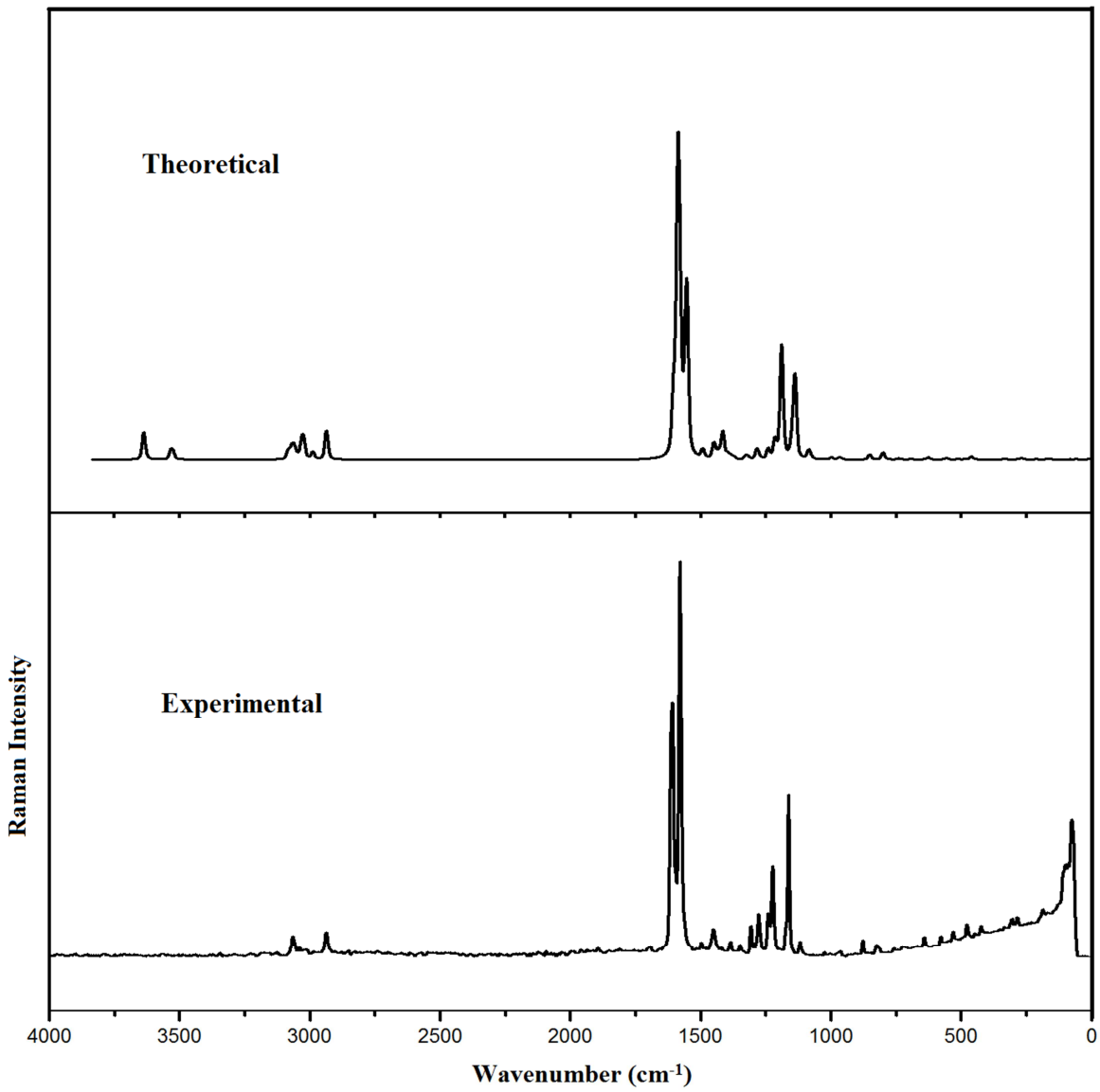

Fig.2 FT-Raman spectrum of 4-[(E)-(4-hydroxybenzylidene)amino]-3-methyl-1H-1,2,4-triazole-5(4H)-thione

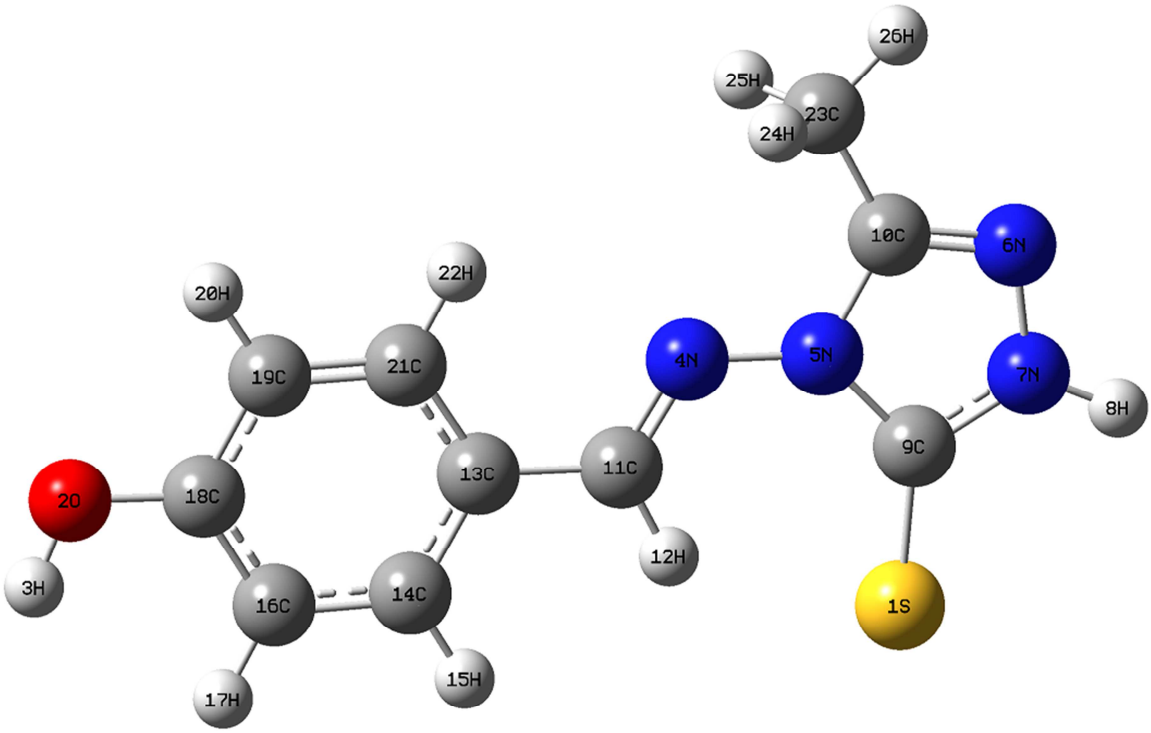

Fig.3 Optimized geometry of 4-[(E)-(4-hydroxybenzylidene)amino]-3-methyl-1H-1,2,4-triazole-5(4H)-thione

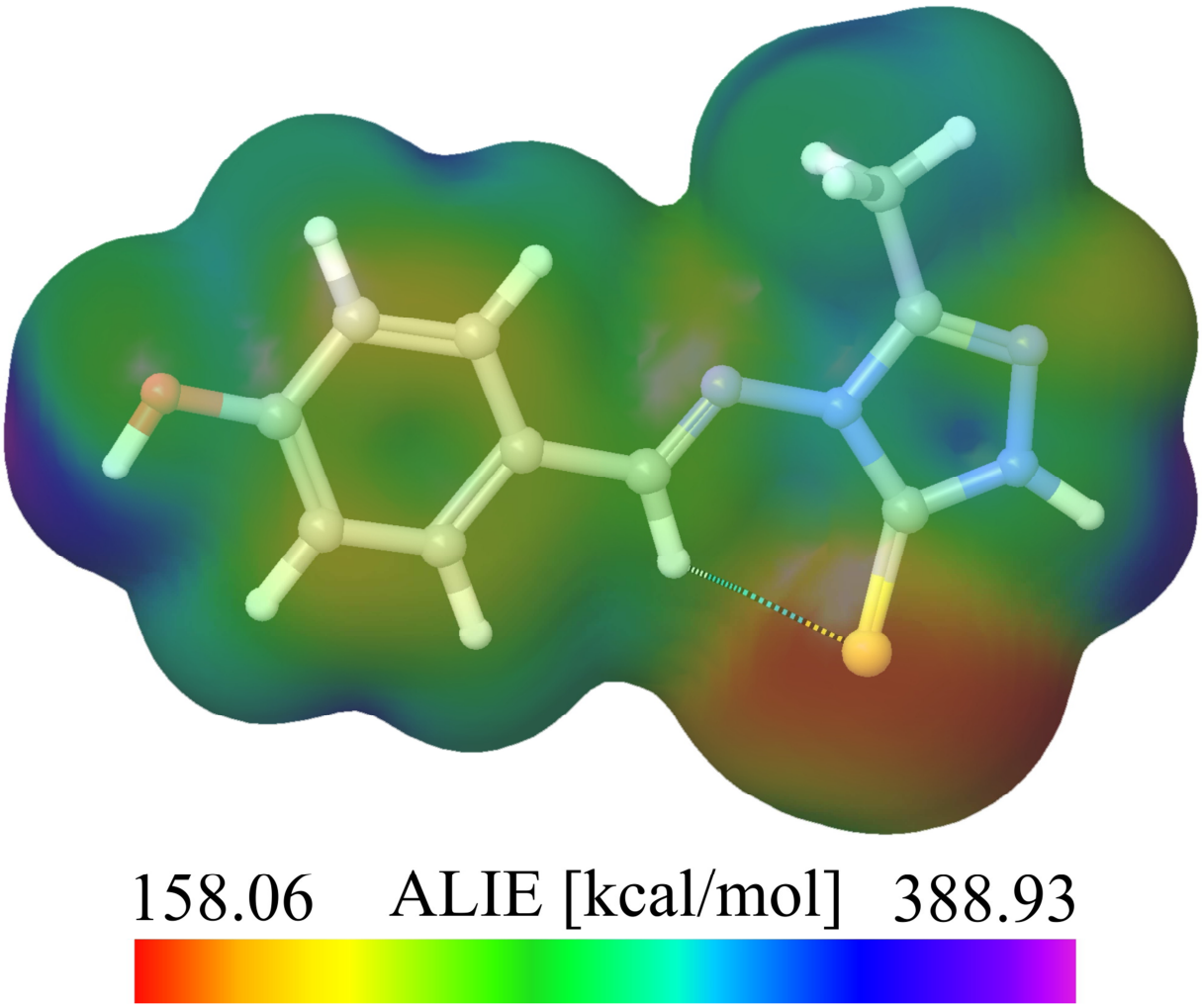

Fig.4 ALIE surface of 4-[(E)-(4-hydroxybenzylidene)amino]-3-methyl-1H-1,2,4-triazole-5(4H)-thione molecule

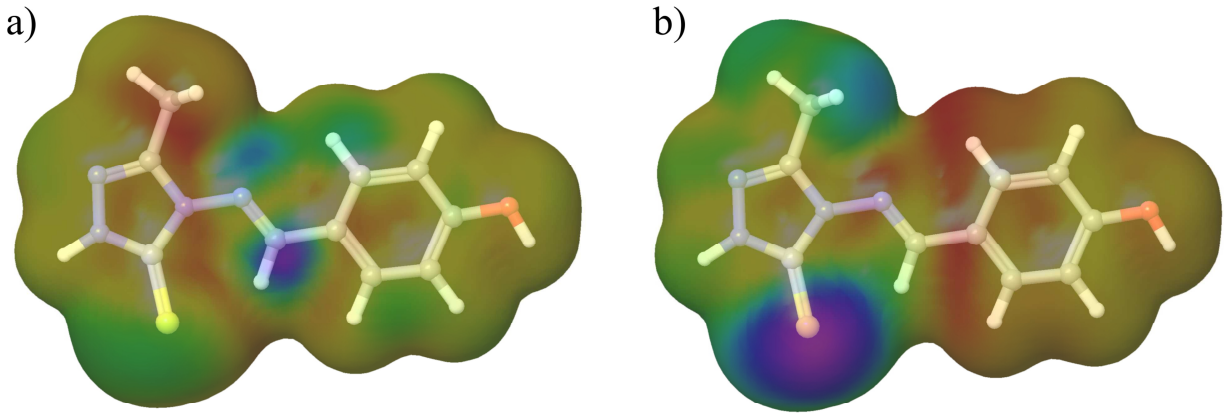

Fig.5 Fukui functions a) f^+ and b) f^- of the 4-[(E)-(4-hydroxybenzylidene) amino]-3-methyl-1H-1,2,4-triazole-5(4H)-thione molecule

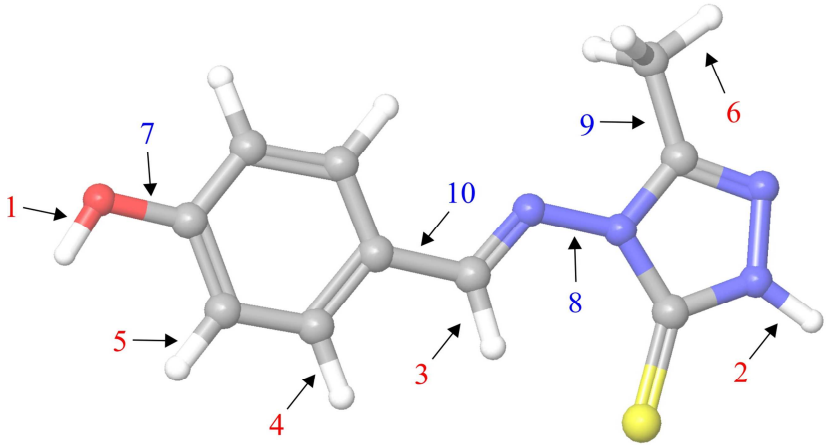

Bond	BDE [kcal/mol]
1	88.62
2	108.43
3	102.57
4	118.02
5	118.10
6	95.29
7	113.21
8	53.80
9	113.89
10	112.54

Fig.6 BDEs of all single acyclic bonds of 4-[(E)-(4-hydroxybenzylidene)amino]-3-methyl-1H-1,2,4-triazole-5(4H)-thione molecule

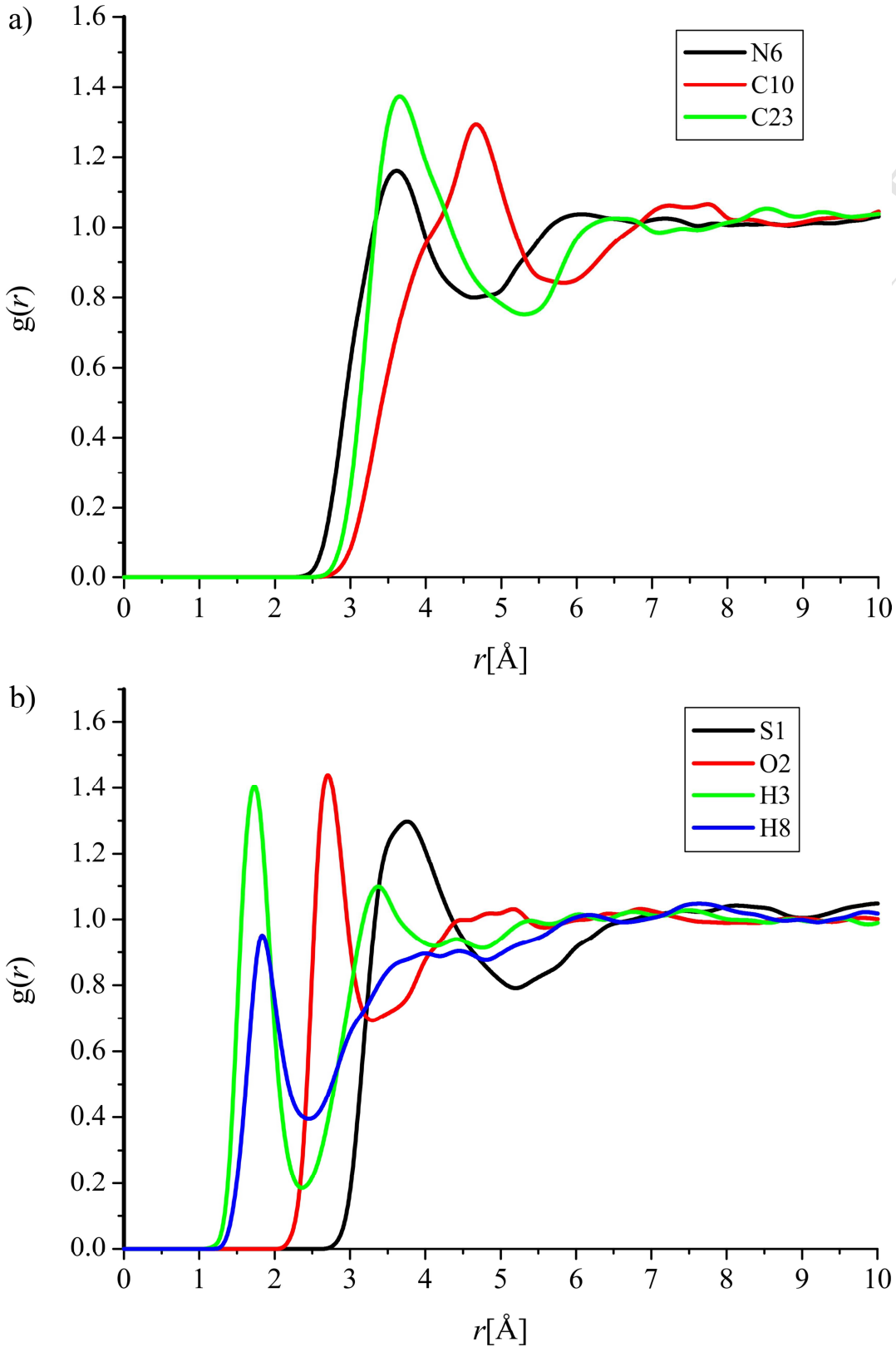

Fig.7 RDFs of atoms of 4-[(E)-(4-hydroxybenzylidene)amino]-3-methyl-1H-1,2,4-triazole-5(4H)-thione molecule with significant interactions with water molecules

Highlights

* IR and Raman spectra were measured
* Most reactive sites are identified
* ALI, BDE, RDF have been discussed in detail
* Title compound forms a stable complex with AChE